pp 1025–1048. © Royal Aeronautical Society 2016
doi: 10.1017/aer.2016.47

Rotorcraft downwash impact on ship airwake: statistics, modelling, and simulation

K. A. Schau

G. Gaonkar
gaonkar@fau.edu
Department of Ocean and Mechanical Engineering
Florida Atlantic University
Boca Raton, Florida
US

S. Polsky
Naval Air Warfare Center Aircraft Division (NAWCAD)
Patuxent River
Maryland
US

ABSTRACT

Helicopter downwash impact on ship airwake is addressed from a three-pronged approach: (1) Analysis of one-point statistics of autospectrum and two-point statistics of cross-spectrum and coherence from a Computational Fluid Dynamics database of flow velocities effected by helicopter downwash and shipboard airwake; (2) Development of a mathematical framework for extracting interpretive turbulence models in closed form from these autospectral statistics; and (3) Simulation through white-noise-driven filters for the extracted models. The framework begins with an earlier-exercised perturbation-type series expansion of the autocorrelation for all three velocity components, where the first term of the series has a form of the von Karman longitudinal or lateral correlation function. After transformation into equivalent series of autospectrum, the coefficients in the series are evaluated by satisfying theoretical constraints and fitting a curve on a set of selected autospectral data points generated from the database. The framework represents a sensible combination of series expansion, exploitation of a database, and theoretical constraints to provide a foothold on airwake-downwash phenomenon for engineering analysis. It ensures that the extracted model and the autospectral data points have the same time scale, mean square value, and asymptotic decay according to the Kolmogorov –5/3 Law. The framework's strengths and weaknesses, and its major advancement over the earlier series-expansion schemes are also addressed. Finally it is shown that downwash increases airwake energy (mean square value) by one order of magnitude, and almost all of this airwake-downwash

Received 29 June 2015; revised 21 January 2016; accepted 4 February 2016; first published online 7 June 2016.

https://doi.org/10.1017/aer.2016.47 Published online by Cambridge University Press

energy is concentrated within the bandwidth $(0.16 < f(Hz) < 1.6)$ that affects flight mechanics.

Keywords: Aerodynamics; turbulence; flight control; flight simulation; rotorcraft; helicopter; downwash; statistics; autospectrum

NOMENCLATURE

A_w	high-frequency spectral decay limit of $f\tilde{S}_{ww}(f)/\sigma_w^2$ (similarly for A_v and A_u) according to Kolmogorov's –5/3 Law
f	frequency (cycle/s or Hz)
$\tilde{R}_{ww}$	modelled series expansion of autocorrelation of turbulence velocity w, (similarly for u and v)
R_{ww} or R_{wPwP}	autocorrelation of vertical turbulence velocity w at a generic point P, first term in the perturbation series expansion of $\tilde{R}_{ww}$, a form of the von Karman vertical correlation function (similarly for R_{uu} and R_{vv})
R_{wPwQ}	cross-correlation between vertical turbulence velocities at P and Q (similarly for u and v)
$\tilde{S}_{ww}$	modelled series expansion of autospectrum of turbulence velocity w, (similarly for u and v)
S_{ww} or S_{wPwP}	autospectrum of vertical turbulence velocity w at P (similarly for u and v)
S_{wPwQ}	cross-spectrum between vertical turbulence velocities at P and Q (similarly for u and v)
S^c_{wPwQ} , S^q_{wPwQ}	co-spectrum and quad-spectrum between vertical turbulence velocities at P and Q (similarly for u and v)
T_u, T_v and T_w	time scales of longitudinal, lateral, and vertical turbulence
t	time (s)
$\bar{u}$, $\bar{v}$ and $\bar{w}$	mean turbulence velocities in the longitudinal, lateral, and vertical directions
u, v and w	turbulence velocities in the longitudinal, lateral, and vertical directions (see Fig. 1)
α_u, α_v, and α_w	scaling or normalisation parameters for autocorrelations (autospectra) of u, v, and w
β_{1w}, β_{2w}, …, β_{nw}	constants in the perturbation series expansion of $\tilde{R}_{ww}$ (see Equation (2a), similarly for $\tilde{R}_{uu}$ and $\tilde{R}_{vv}$)
γ^2_{wPwQ}	coherence or coherence function between vertical turbulence velocities w_1 at P and w_2 at Q (similarly for γ^2_{uPuQ} and γ^2_{vPvQ})
θ_{wPwQ}	phase angle of cross-spectrum $\tilde{S}_{wPwQ}$ (similarly for θ_{uPuQ} and θ_{vPvQ})
σ_w	root mean square (rms) of vertical turbulence velocity (similarly for σ_u and σ_v)
σ_w^2	variance or energy of vertical turbulence velocity (see Equation (2c), similarly for σ_u^2 and σ_v^2)
τ	time interval or time lag, t_2 - t_1,

https://doi.org/10.1017/aer.2016.47 Published online by Cambridge University Press

1.0 INTRODUCTION

Helicopter shipboard operations have to contend with airwake-downwash turbulence: the coupled flow-field of ship's airwake shed from the superstructure and the thrust-induced downwash from the helicopter itself[1]. Airwake-downwash turbulence is formidably complex in that it is nonhomogeneous and rapidly distorting. Due to this complexity, the current predictive capability for the autospectrum and such fundamental statistics merits significant improvement, let alone the capability for real-time simulation. Over the past five years, the state of the art of treating airwake-downwash turbulence in the helicopter-ship dynamic interface has been thoroughly reviewed by Ref. 2, and a summary account is given by Refs 3, 4 and 5. As seen from these studies[2–5], major strides have been made in generating the database of flow velocity points, primarily based on CFD approaches and, to a lesser degree, based on wind-tunnel and full-scale experiments.

This database presents an unharnessed opportunity for generating a relatively complete set of statistics and developing interpretive models. Specifically, the statistics refer to one-point statistics of autospectrum for all three velocity components and to the corresponding two-point statistics of cross-spectrum and coherence. The interpretive models[5] represent these one-point statistics in closed form. By design, they have a simple analytical structure to facilitate delineation, simulation through white-noise-driven filters and routine use as a predictive tool. Because of the built-in simplicity, they offer considerable promise for real-time simulation. Moreover, they broaden the scope and utility base of a database that invariably requires enormous resources. The present paper is driven by this opportunity.

The mathematical framework for developing interpretive autospectral models from a database posits that airwake-downwash turbulence is nonlinearly transformed atmospheric boundary layer turbulence (ABL); see Ref. 5. Specifically, each velocity component is treated independently of the other, each component having its own time scale and rms value. Classical homogeneous, isotropic turbulence theory along with Taylor's frozen turbulence hypothesis[1] is adapted to modelling ABL. With this adaptation, the autocorrelation for each component is represented by a separate perturbation-type series in which the first term has a form of the von Karman longitudinal or lateral correlation function. After transformation into equivalent perturbation series of autospectrum, the coefficients in the series are calculated by satisfying the theoretical constraints and fitting a curve to a set of selected autospectral data points on a least squares basis. The framework represents a judicious combination of a mathematical formulation based on series expansion, a database, and theoretical constraints. In turn, it guarantees that, for all three velocity components, the extracted autospectral models and the corresponding autospectral data points have the same time scale, mean square value and asymptomatic decay according to the Kolmogorov $-5/3$ Law[5]. That is, all three fundamental turbulence characteristics of the data are captured by the extracted models.

Harris was the first to propose that the longitudinal autocorrelation function of nonlinearly transformed ABL can be expressed by a perturbation-type series[6]. For some assumed values of constants in the series expansion, he qualitatively showed the utility of this approach for modifying the von Karman longitudinal autospectrum to include autospectral variation with height above the ground[6]. Here, the focus is almost exclusively on the longitudinal component, for which, the treatment also includes two constraint equations in closed form, which are related to the preservation of time scale and asymptotic decay. In Harris' treatment, the lateral and vertical autospectra are derived from the longitudinal by invoking the continuity equation for an incompressible fluid. A direct extension of this work to nonhomogeneous, non-isotropic turbulence leads to inconsistent and arbitrary time scales. Harris' work does not

https://doi.org/10.1017/aer.2016.47 Published online by Cambridge University Press

address any application to a database. Despite all this, the pioneering treatment of Harris sets the stage for exploiting the potentialities of the series-expansion approach and the database.

In a recent study[7], the treatment of Harris has been extended to modelling ship airwake. Here, the focus is on autospectral and cross-spectral models in the low-frequency bandwidth ($0 \leq f\ (Hz) \leq 1.6$). More important, the approach of Ref. 7 is completely numerical, and it does not provide a means of preserving the key turbulence characteristic of autospectral asymptomatic decay in the extracted model. Reference 8 is another follow-up study, which represents a preliminary investigation of helicopter downwash effects on ship airwake with the approach of Ref. 7.

Now, it is expedient to ask: How far does this work advance the state of the art of treating airwake with downwash, particularly as an advancement over the works of Harris[6] and Gaonkar and Mohan[7]? For the first time, this paper exploits a comprehensive database – airwake alone, downwash alone, and airwake with downwash – to generate one-point statistics of autospectrum and two-point statistics of cross-spectrum and coherence. Thereby, it demonstrates the impact of downwash-induced disturbances on the entire flow-field of airwake. Above the rotor plane, these disturbances directly affect the rotor; as excitations to the rotor itself, they are critical to low-speed helicopter flight dynamics. Below the rotor plane, these disturbances, as internal excitations from the rotor to the fuselage, increase the fuselage loads and in turn affect the pilot's workload and operational envelope[9,10].

In developing a mathematical framework as well, while the present study[5] is built on the works of Harris[6] and also Gaonkar and Mohan[7], it expands on them in three respects. First, for time scale preservation and asymptotic decay, it derives from first principles the constraint equations in closed form for the vertical component. These equations also apply to the lateral component with only minor changes. Second, it refines the formulation of Gaonkar and Mohan[7] to include the constraint equations for all three velocity components, so that the extracted autospectral models capture asymptotic decay and such fundamental characteristics of the autospectral data points. Third, it demonstrates that the framework is robust and that the extracted models lend themselves well to designing shaping filters driven by white noise. This demonstration is based on a comprehensive database of airwake with downwash.

2.0 MODEL STRENGTHS AND WEAKNESSES

Airwake-downwash turbulence deviates appreciably from ABL, whereas the framework is based on a perturbation-type series expansion in which the first term is represented by a form of the von Karman autocorrelation function from classical turbulence theory, including Taylor's hypothesis[1]. Moreover, there is no guarantee that the contribution of the first term of the series dominates over those of the second and remaining terms. These concerns should be tempered with the intended role of the framework: To provide a foothold on airwake-downwash phenomenon for engineering analysis. Moreover, the framework does not follow the classical perturbation theory approach of a linearised solution with perturbation corrections as add-ons. In fact, it represents a practical combination of series expansion, exploitation of the database, and theoretical constraints, and thereby it guarantees that time scale, mean square value and asymptomatic decay of the autospectral data points are preserved in the extracted models. It is emphasised that Taylor's hypothesis and the Kolmogorov –5/3 Law are found to be remarkably robust[11,12]. It is further emphasised that Taylor's hypothesis is not restricted to homogeneous turbulence and that this hypothesis is applicable to all turbulent flows as long as mean flow velocity is larger, compared to the eddy convection

https://doi.org/10.1017/aer.2016.47 Published online by Cambridge University Press

velocity[11,12]. "Thus, in practice, although Taylor's hypothesis is not exact, because real turbulence evolves as it is convected, it is approximately true in many flows[11]." While the validity of Taylor's hypothesis for airwake-downwash turbulence may be debatable, this hypothesis provides a powerful means of converting spatial coordinates into temporal coordinates. And the Kolmogorov –5/3 Law is well supported by experiments in a variety of flow fields, ranging from tidal flows and atmosphere near the sea surface to wind-farm wake turbulence and ship airwake with and without downwash[5,11]. This Law requires, though, high-Reynolds-number and fully-developed-turbulence conditions[11]. By design, the construction of shaping filters driven by white noise is as routine as the currently used procedure for the von Karman. What is more, the framework's utility is well borne out when tested against a comprehensive CFD database (details to follow). As things turn out, these models typically require no more than a first-order correction (a two-term series).

These weaknesses notwithstanding, this work should serve as a reference point for future investigations of downwash effects on the helicopter-ship dynamic interface. After all, almost all aspects of this interface, from pilot workload to excitations to the rotor/fuselage system to health and safety concerns, are affected by downwash coupling with airwake, not to mention the launch and recovery envelope[10].

3.0 DOWNWASH-IMPACT STATISTICS

The stochastic description is based on one-point statistics of autospectrum and two-point statistics of cross-spectrum and coherence. These statistics for airwake with downwash are compared with the corresponding statistics for airwake alone, and this comparison is used to quantify the impact of downwash on airwake. For all these results, the database lays the groundwork. Accordingly, it is presented first.

3.1 Database

The database is CFD-based and it was generated at the Naval Air Warfare Center Aircraft Division (NAWCAD), Patuxent River, Maryland. Specifically, it refers to flow velocity points of airwake for a DDG-81 Class Ship at rest with a 25-Kn headwind. Downwash coupling is simulated through an embedded H-60 actuator disk model (the rotors of Sikorsky SH-60 (Sea Hawk) and S-70 (Black Hawk) are virtually identical, and they are commonly referred to as H-60 rotor). Simply put, the flow field comprises the airwake shed by a 25-Kn headwind and downwash from an H-60 rotor hovering within this airwake.

The database is voluminous. Velocity data exists at 258,335 points in space that are arranged in a three-dimensional spatial grid of 55 $\times$61 $\times$77 nodes. The grid begins at what could be considered as the landing area and propagates back over 400 feet behind the ship. In total, 600 flow velocity predictions spaced at 0.1 seconds apart (1 minute of transient data) are available at each of these 258,335 points. The H-60 actuator disk model is embedded at 20 representative locations within the grid, and a complete set of flow velocity data are available for each of these 20 locations. To sum up: a total of 258,335 $\times$600 $\times$3 $\times$20 data points; that is, well over 9.3 Bn velocity points of airwake with downwash.

The database is also comprehensive in that it comprises two equally compelling sets of data points: one for the 25 Kn airwake alone and one for downwash alone, under identical conditions (in the airwake-alone case the actuator disk is absent; in the downwash-alone case the headwind is absent) Thus, it provides a direct means of isolating and quantifying downwash impact on airwake.

https://doi.org/10.1017/aer.2016.47 Published online by Cambridge University Press

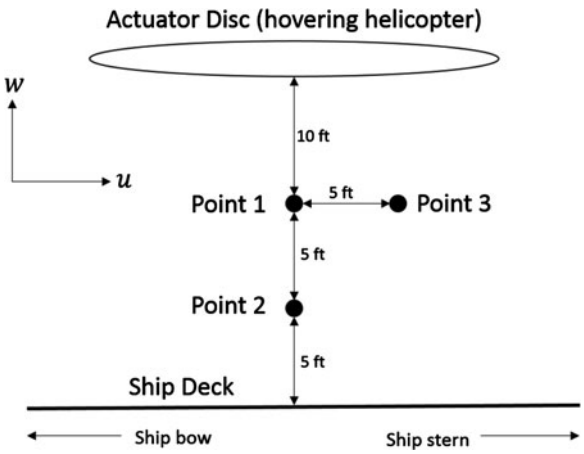


Figure 1. A schematic of topology of point one, point two, and point three in the spatial grid relative to the actuator disk and deck level.

3.2 One-Point and Two-Point Statistics

Given the extent of the database, the statistics are presented for three points in the spatial grid, which are schematically shown in Fig. 1, along with the topology relative to the actuator disk and landing deck. The first two points are 10 feet and 15 feet vertically below the actuator disk, and the third point is 5 feet horizontally to the right from the first. In the sequel, these three points are referred to as 'Point One', 'Point Two', 'Point Three', and the actuator disk is referred to as a "hovering helicopter".

Figure 2 refers to Point One, and Fig. 3 to Point Two, 10 feet and 15 feet vertically below a hovering helicopter, respectively. Each of two figures presents how the autospectra of longitudinal, lateral, and vertical components for airwake with downwash compare with the corresponding autospectra for airwake alone. This comparison is of significance in that the area under dimensional $S_{ii}(f)$ versus f curve represents the mean square σ_i^2, which is also referred to as turbulence energy in the sense that σ_i^2 also represents variance (because the mean flow is subtracted from the velocity time history). Moreover, the frequency bandwidth over which this energy is concentrated can be identified as well. For illustration, the vertical component at Point One in Fig. 2 is considered. The energy, or mean square σ_{W1}^2, is 31.00 (m^2/s^2) without downwash, compared to 304.4 (m^2/s^2), with downwash, nearly a tenfold increase due to downwash coupling. Equally important, almost all of this energy is concentrated within the low-frequency bandwidth $(0.16 \leq f\ (Hz) \leq 1.6)$ that is of concern to helicopter flight mechanics. The results of Fig. 3 exhibit the same pattern, that is, one order of magnitude increase of turbulence energy because of downwash coupling: $\sigma_{W2}^2 =$ 242.9 (m^2/s^2) with downwash compared to 15.00 (m^2/s^2) without downwash, nearly a 16-fold increase (the autospectral and mean square results for Point Three (Fig. 1) essentially depict the same trend and are thus omitted).

Compared to the preceding consideration of airwake-downwash turbulence energy and its concentration over a low-frequency bandwidth, the asymptotic decay of autospectra is more subtle. And, it is equally significant from the consideration of whether the turbulence flow field is still distorting or close to be being fully developed. As seen from Figs. 2 and 3, the asymptotic decay rate for all three velocity components of airwake with downwash is a bit

https://doi.org/10.1017/aer.2016.47 Published online by Cambridge University Press

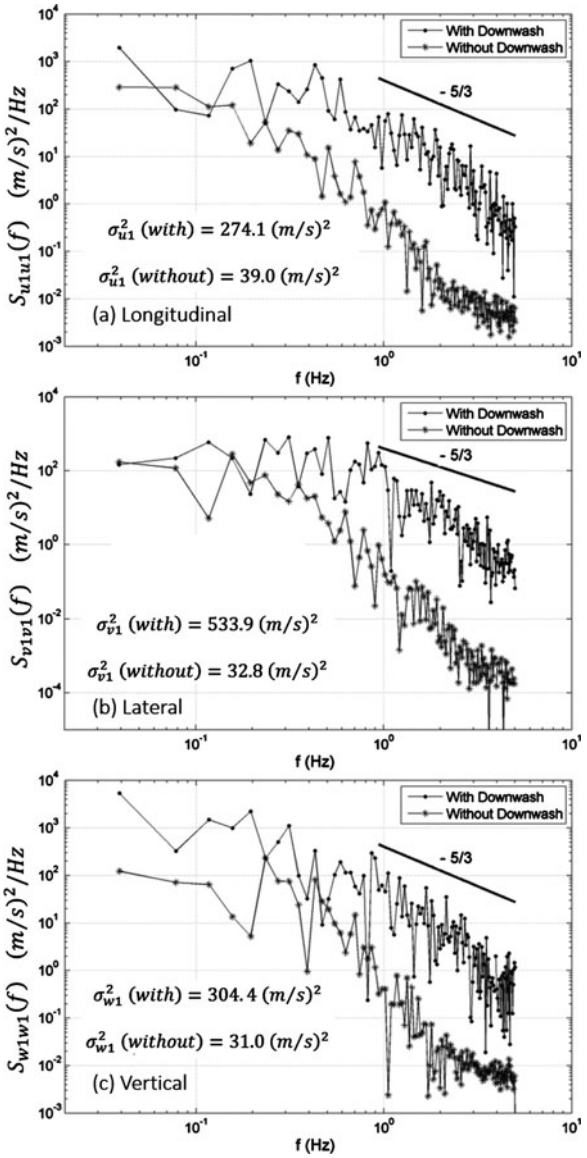


Figure 2. Autospectra with and without downwash at point one, 10 feet vertically below a hovering helicopter.

higher than the Kolmogorov –5/3 decay rate, and for airwake alone, the decay rate is fairly comparable to the Kolmogorov rate. Observe that the Kolmogorov Law of –5/3 autospectral asymptomatic decay requires high-Reynolds-number and fully developed turbulence. Thus, this steeper-than-the-Kolmogorov decay rate due to downwash coupling seems to indicate that, compared to airwake alone, airwake with downwash is relatively less fully developed; that is, the eddy distortions are more pronounced and they continue longer. These remarks on the Kolmogorov decay rate, however, merit revisiting on the basis of experimental, at-sea or wind-tunnel data.

https://doi.org/10.1017/aer.2016.47 Published online by Cambridge University Press

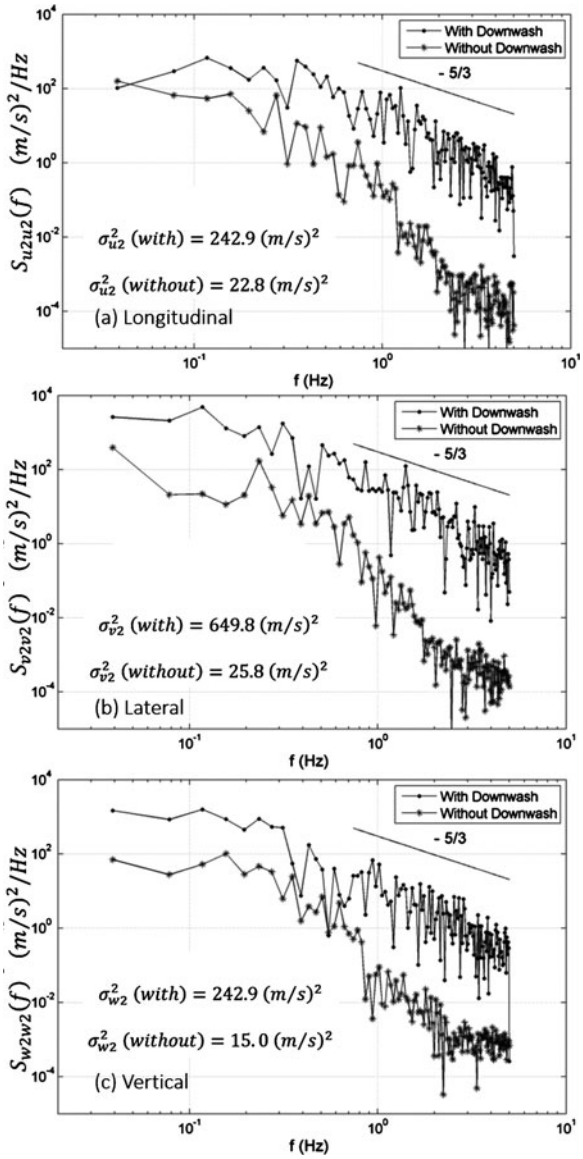


Figure 3. Airwake autospectra with and without downwash at point two, 15 feet vertically below a hovering helicopter.

Figures 2 and 3 show the impact of downwash on the airwake flow field. The CFD database offers a set of data in which airwake is not present in the flow field, leaving downwash as the driving factor. Figure 4 shows the autospectral results from this downwash-only flow field at Point One, plotted with the coupled autospectra of Fig. 2. As expected, downwash is the driving factor in that the two spectra are virtually indistinguishable. Here as well, further research is required on the basis of experimental data.

https://doi.org/10.1017/aer.2016.47 Published online by Cambridge University Press

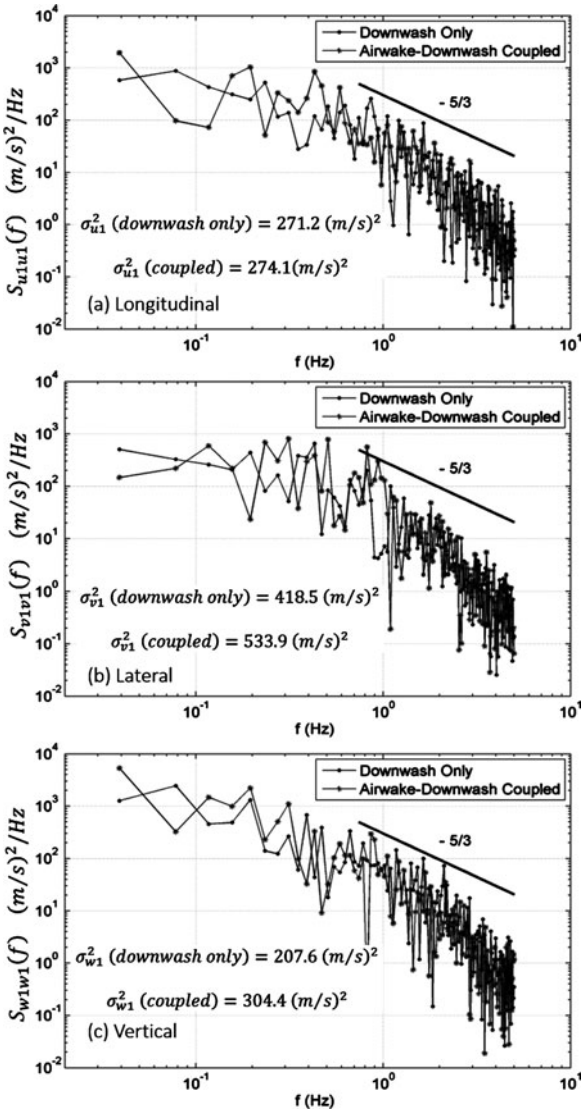


Figure 4. Airwake-downwash autospectra and downwash-only autospectra at point one, 10 feet vertically below a hovering helicopter.

The next set of statistics on the impact of downwash on airwake represents the two-point statistics of cross-spectrum and coherence. To help present the results without any ambiguities of terminologies, and to appreciate the results, the basic equations of the two-point statistics of cross-spectrum and coherence are first mentioned in passing, and then the results are presented. The correlation between, say vertical component $w_1(t)$ at Point One and $w_2(t+\tau)$ at Point Two, for the time interval τ is the cross-correlation $R_{w1w2}(\tau)$. The Fourier transform of $R_{w1w2}(\tau)$ is the cross-spectrum, which is a complex valued function[13]:

$$S_{w1w2}(f) = S^c_{w1w2}(f) - i\, S^q_{w1w2}(f) = |S_{w1w2}(f)|\; e^{-i\theta_{w1w2}}, \qquad \ldots (1a)$$

https://doi.org/10.1017/aer.2016.47 Published online by Cambridge University Press

where $S^{c}_{w1w2}(f)$ is the co-spectrum, $S^{q}_{w1w2}(f)$ is the quad-spectrum, and θ_{w1w2} is the phase angle. Specifically, the magnitude and phase are given by

$$|S_{w1w2}(f)| = \sqrt{\left[S^{c}_{w1w2}(f)\right]^2 + \left[S^{q}_{w1w2}(f)\right]^2}, \quad \ldots(1b)$$

$$\theta_{w1w2} = \tan^{-1}\left(\frac{S^{q}_{w1w2}(f)}{S^{c}_{w1w2}(f)}\right), \quad \ldots(1c)$$

Given the autospectra for both $w_1(t)$ and $w_2(t)$ – $S_{w1w1}(f)$ and $S_{w2w2}(f)$ – and the magnitude of the cross-spectrum between $w_1(t)$ and $w_2(t)$ – $|S_{w1w2}(f)|$ – the corresponding coherence or coherence function (also referred to as the *spectral correlation coefficient*) is given by[13]

$$\gamma^2_{w1w2}(f) = \frac{|S_{w1w2}(f)|^2}{S_{w1w1}(f)\,S_{w2w2}(f)} \quad , \quad 0 \le \gamma^2_{w1w2}(f) \le 1 \quad \ldots(1d)$$

As expected, for $w_1(t) = w_2(t)$, $\gamma^2_{w1w2}(f) = 1$ represents perfect correlation. Coherence $\gamma^2_{w1w2}(f)$ is greater than zero and less than one, and this shows the extent to which these two series are "similar" or correlated at each frequency.

For both airwake and airwake-downwash turbulence, Fig. 5 shows the cross-spectrum $S_{w1w2}(f)$ between the vertical components $w_1(t)$ at Point One and $w_2(t)$ at Point Two; magnitude, as typified by Equation (1b), is shown in Fig. 5(a), and phase, as typified by Equation (1c), in Fig. 5(b). As seen from Fig. 5(a), downwash impact on airwake is severe for both points; that is, airwake-downwash turbulence within the area containing both points has more energy than airwake for the entire frequency range. The phase information in Fig. 5(b) is extremely instructive in comparison to some of the extensively pursued nonhomogeneous, anisotropic flow fields. As an illustration, for ABL near the ground, the phase angle is found to be relatively small and thus, the cross-spectrum is often approximated by the real part or co-spectrum; see Ref. 14 for details. By contrast, Fig. 5(b) shows that, for both airwake and airwake-downwash turbulence, the widely used small-phase approximation, that is, approximating cross-spectrum by its real part co-spectrum, is not tenable. For a relatively complete picture of two-point statistics in the interface, the cross-spectrum between point one and point three – $S_{w1w3}(f)$ – is also included in Fig. 6, magnitude in Fig. 6(a), and phase in Fig. 6(b). Here as well, the overall impact of downwash on airwake on the basis of cross-spectrum magnitude and phase variation with frequency is similar to that of $S_{w1w2}(f)$ in Fig. 5. The cross-spectral results for the longitudinal and lateral components are essentially similar to those of the vertical components and are thus omitted.

Figure 7 shows coherences $\gamma^2_{w1w2}(f)$, $\gamma^2_{w1w3}(f)$, and $\gamma^2_{w2w3}(f)$ for vertical velocity components for three pairs of points; also see Fig. 1. For example, $\gamma^2_{w1w2}(f)$ represents the dimensionless correlation between vertical components $w_1(t)$ at Point One and $w_2(t)$ at Point Two in the frequency domain; this should explain why coherence, as typified by Equation (1d), is also referred to as the spectral correlation coefficient. Coherence is widely used as a quantitative measure of similarity (or dissimilarity) between two time histories of flow velocities[13]. As seen from Fig. 7, for airwake-downwash turbulence, the coherence is generally low (*say* $\gamma^2_{ii} < 0.5$) for all three velocity components for most of the entire bandwidth ($0 \le f\,(Hz) \le 5$); this indicates that the two time histories of the

https://doi.org/10.1017/aer.2016.47 Published online by Cambridge University Press

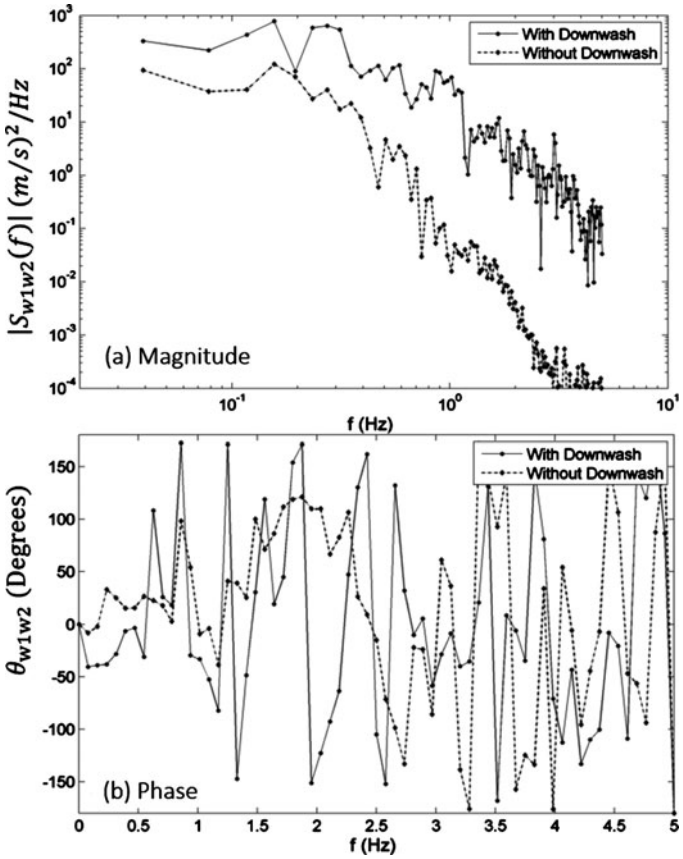


Figure 5. Airwake vertical cross-spectrum with and without downwash between point one and point two (these two points are identified in Fig. 1).

corresponding components at these two points are weakly correlated. By comparison, the coherence values are much higher ($\gamma_{ii}^2 > 0.5$) for airwake alone; that is, the correlation between the corresponding time histories is relatively stronger. These comparative features are consistent with the physics of two flow fields. Compared to airwake, airwake-downwash turbulence is far more distorting with reduced point-to-point similarity because of downwash coupling.

As seen from Fig. 1, all three points, thus far investigated, are below the rotor plane, two points vertically down and the third one slightly behind the rotor. Although significant in the prediction of downwash-induced fuselage loads and the corresponding impact on pilot work load and operational envelope[9,10], flow disturbances at these below-the-rotor-plane points represent an excitation that is internal to the rotor-fuselage system: from the rotor to the fuselage. By comparison, flow disturbances at points upstream of the rotor and above the rotor plane convect downstream and directly impact the rotor as an excitation to the rotor itself; and this excitation is thought to have a major effect on low-speed helicopter flight dynamics. That is, this excitation (rather than fuselage forces) is the primary source of pilot workload and limitations. Accordingly, one point just upstream of the rotor, and two points above the rotor are selected (these points are not shown). Specifically, the upstream point is on the rotor plane

https://doi.org/10.1017/aer.2016.47 Published online by Cambridge University Press

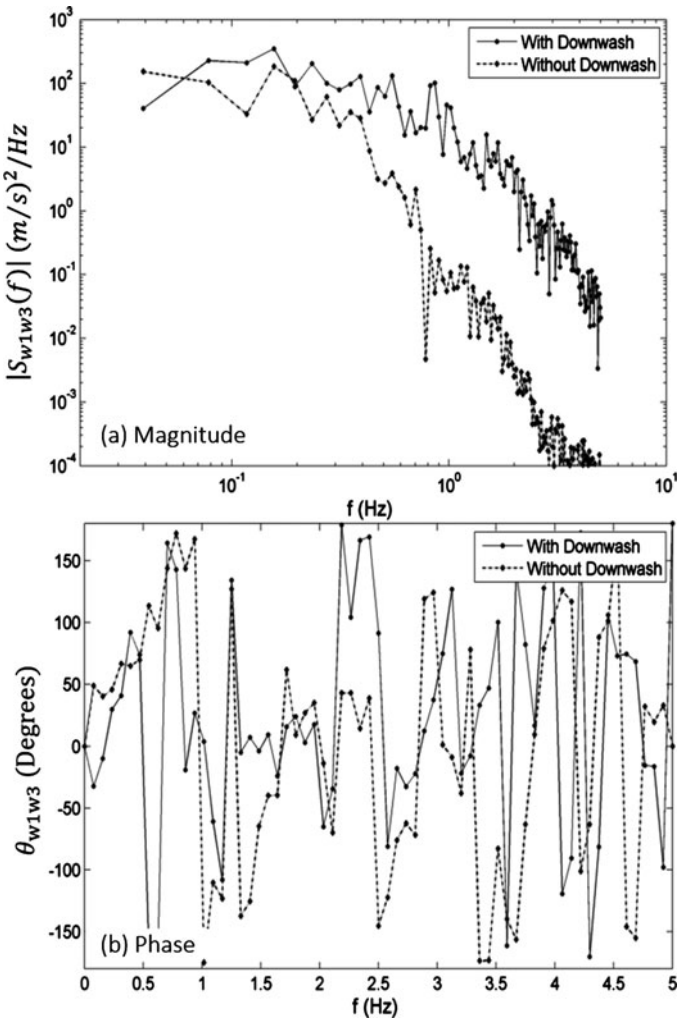


Figure 6. Airwake vertical cross-spectrum with and without downwash between point one and point three (these two points are identified in Fig. 1).

and 10 feet forward of the rotor, and the other two points are 5 feet and 10 feet vertically above the rotor. For quantitative illustration, suffice it to consider σ_w^2, the energy values of the vertical components of airwake alone and airwake with downwash. Because of downwash, σ_w^2 increases threefold at the point 5 feet vertically above, and 40% at the upstream point on the rotor plane and marginally at the point 10 feet vertically above. Finally, it is also instructive to compare downwash effects at two "representative points" that are above and below the rotor plane, say at Point One (Fig. 1), 10 feet vertically below the rotor and at another point, 5 feet vertically above. At Point One, σ_w^2 increases tenfold from downwash and at the latter point, it increases threefold. The message is that, while downwash effects vary from point to point, these effects should be included in any realistic assessment of how the flow-field affects the vehicle.

https://doi.org/10.1017/aer.2016.47 Published online by Cambridge University Press

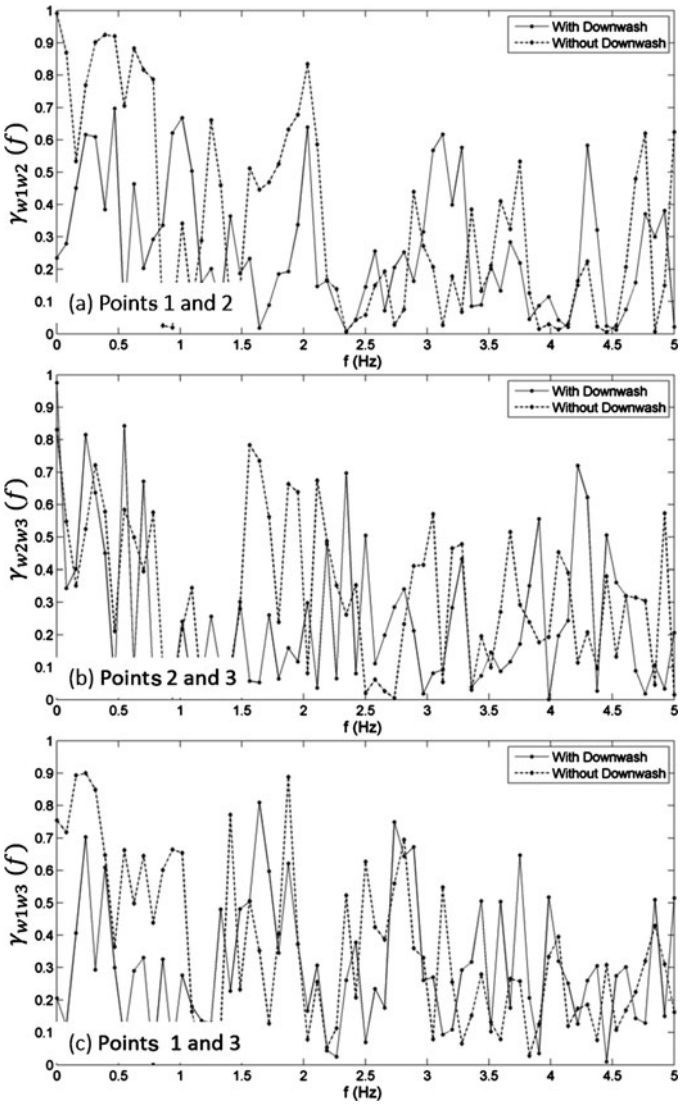


Figure 7. Vertical airwake coherences with and without downwash for three pairs of points (these three points are identified in Fig. 1).

4.0 MATHEMATICAL FRAMEWORK

The mathematical framework represents the series expansion approach in combination with the theoretical constraints and a database so that the extracted autospectral model from this database and the autospectral data points have the same time scale, mean square value, and asymptotic decay. The contributions of this paper are novel in three respects: (1) Derivation of theoretical constraints of time scale and asymptotic decay in closed form for the vertical component (essentially the same constraints apply to the lateral component with minor changes); (2) Development of a framework with built-in theoretical constraints for all three

https://doi.org/10.1017/aer.2016.47 Published online by Cambridge University Press

components (the constraints for the longitudinal were derived earlier by Harris[6]); and (3) Demonstration of the framework's viability against a comprehensive database.

For illustration, the vertical velocity component $w(t)$ of airwake-downwash turbulence is selected; therein, the mean value $\bar{w}(t)$ plus the corresponding fluctuation or turbulence $w(t)$ represent the total vertical component: $w(t) + \bar{w}(t)$. For the longitudinal and lateral components, the details run virtually parallel to those of the vertical. Moreover, for helicopter flight dynamics applications, the vertical component is generally more important than the other two components.

4.1 Vertical Turbulence Model

The autocorrelation of vertical airwake-downwash turbulence $\tilde{R}_{ww}(\tau)$ is expressed by a perturbation-type series:

$$\tilde{R}_{ww}(\tau) = \beta_{1w} R_{ww}(\tau) + \beta_{2w} R^2_{ww}(\tau) + \cdots + \beta_{nw} R^n_{ww}(\tau) \quad \ldots (2a)$$

Using the classical definition of time scale $T_w = \int_0^\infty \tilde{R}_{ww}(\tau) d\tau$ and with $\tilde{S}_{ww}(f)$ representing the vertical airwake-downwash turbulence autospectrum, Equations (2b) and (2c) provide the footholds for the derivation of the constraint equations.

$$\tilde{S}_{ww}(0) = 4\sigma_w^2 \int_0^\infty \tilde{R}_{ww}(\tau)\, d\tau = 4\sigma_w^2 T_w, \quad \ldots (2b)$$

$$\frac{1}{\sigma_w^2} \int_0^\infty \tilde{S}_{ww}(f)\, df = \tilde{R}_{ww}(0) = 1, \quad \ldots (2c)$$

where σ_W^2 is the mean square value, or variance. Furthermore, $R_{ww}(\tau)$, the first term on the right side of Equation (2a), is referred to here as a basis function, and it is represented by a form of the von Karman vertical correlation function:

$$R_{ww}(\tau) = \frac{2^{2/3}}{\Gamma\left(\frac{1}{3}\right)} \left(\frac{\alpha_w \tau}{T_w}\right)^{1/3} \left[K_{1/3}\left(\frac{\alpha_w \tau}{T_w}\right) - \frac{1}{2}\left(\frac{\alpha_w \tau}{T_w}\right) K_{2/3}\left(\frac{\alpha_w \tau}{T_w}\right)\right], \quad \ldots (2d)$$

where α_w is introduced to satisfy Equation (2b) and serves as a time-scale preservation parameter. $K_{1/3}$ and $K_{2/3}$ are modified Bessel functions of order 1/3 and 2/3, respectively; this is necessitated by the definition of autocorrelation, $\tilde{R}_{ww}(0) = 1$, regardless of the value of α_w. As seen from Equations (2a) and (2d), β_{1w}, β_{2w}, $\ldots$, β_{nw} along with α_w, represent n+1 unknown constants. Their evaluation requires the autospectrum, which is obtained by taking the Fourier transform of Equation (2a):

$$\tilde{S}_{ww}(f) = \beta_{1w} S_{ww1}(f) + \beta_{2w} S_{ww2}(f) + \cdots + \beta_{nw} S_{wwn}(f), \quad \ldots (3)$$

where $S_{wwn}(f)$ is the Fourier transform of $R^n_{ww}(\tau)$. A part of Fig. 8 shows the corresponding Fourier transforms multiplied by f: $fS_{ww1}(f)$, $fS_{ww2}(f)$, and $fS_{ww3}(f)$ (i.e. the terms of Equation (3) if all beta coefficients are set to unity).

https://doi.org/10.1017/aer.2016.47 Published online by Cambridge University Press

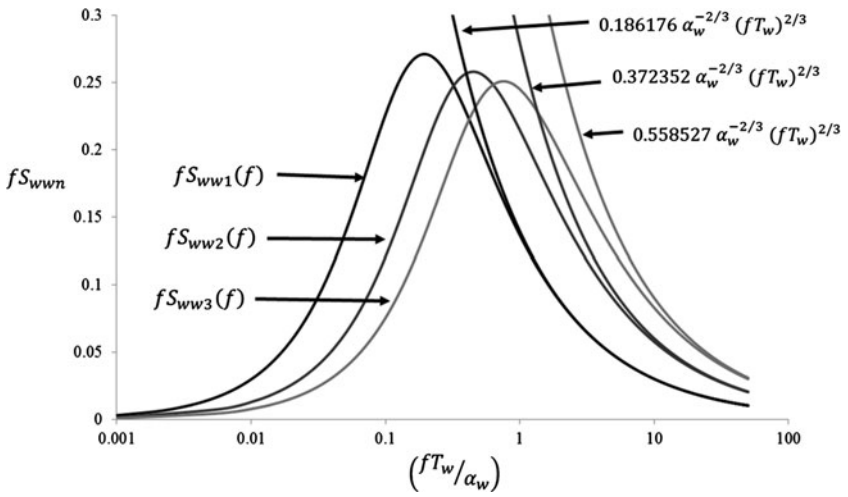


Figure 8. A geometrical representation of asymptotic decay according to the Kolmogorov –5/3 law.

4.2 Constraint Equations

Since $\tilde{R}_{ww}(0) = R_{ww}(0) = 1$, Equation (2a) gives

$$\beta_{1w} + \beta_{2w} + \cdots + \beta_{nw} = 1 \qquad \ldots (4a)$$

Integrating Equation (2a), and using the relation in Equation (2b) lead to[5]:

$$\alpha_w = \beta_{1w} \int_0^\infty R_{ww}(\tau)\, d\tau + \beta_{2w} \int_0^\infty R_{ww}^2 d\tau + \cdots + \beta_{nw} \int_0^\infty R_{ww}^n d\tau \qquad \ldots (4b)$$

$$\alpha_w = \frac{\sqrt{\pi}\,\Gamma\left(\frac{5}{6}\right)}{2\,\Gamma\left(\frac{1}{3}\right)} \left[\beta_{1w} + \beta_{2w}\frac{79\sqrt{3}}{256} + \beta_{3w} \times D\right], \qquad \ldots (4c)$$

where D is evaluated numerically. Finally,

$$\alpha_w = 0.373417\,\beta_{1w} + 0.199591\,\beta_{2w} + 0.122360\,\beta_{3w} \qquad \ldots (4d)$$

Similarly, the Kolmogorov asymptotic Law requires[5]:

$$\left[\frac{f\,S_w(f)}{{\sigma_w}^2}\right]_{\text{high frequency}} = A_w (f\,T_w)^{-2/3} \qquad \ldots (5a)$$

After some manipulations, Equation (5a) reduces to

$$\frac{A_w}{\alpha_w^{2/3}} = \frac{16}{3(2\pi)^{5/3}} \frac{\sqrt{\pi}\,\Gamma\left(\frac{5}{6}\right)}{\Gamma\left(\frac{1}{3}\right)} [\beta_{1w} + 2\beta_{2w} + 3\beta_{3w} + \cdots], \qquad \ldots (5b)$$

https://doi.org/10.1017/aer.2016.47 Published online by Cambridge University Press

where A_w is the asymptotic value, which is extracted from the autospectral data points according to Equation (5a)[5]. This equation is simplified to:

$$\frac{A_w}{\alpha_w^{2/3}} = 0.186176\,\beta_{1w} + 0.372352\,\beta_{2w} + 0.558527\,\beta_{3w} \qquad \ldots (5c)$$

Figure 8 shows a geometrical representation of Equation (5c); for additional details, see Ref. 5. The closed form expressions, as typified by Equations (4a), (4c), and (5b), represent the constraint equations of the model framework.

5.0 NUMERICAL ASPECTS

The process of managing the voluminous database and generating the autospectral data points, and then evaluating the unknowns in the series expansion, involves many and varied details[5]. The following account is intended to convey a flavor of this process; although addressed for the vertical component, it applies to the other two components as well. As seen from Equations (2a) and (2d), the numerical task boils down to computing 'n' series-expansion constants of β_{1w}, β_{2w}, β_{3w}, and one normalisation parameter α_w. The task begins with the evaluation of the mean square value σ_w^2 directly from the raw data points. Then, the autospectral data points, including the point at zero frequency, are generated from the database, and the mean square value σ_w^2 is once again evaluated from Equation (2c); these two sets of mean square values are found to agree fairly well. Finally, the time scale T_w is calculated from Equation (2b), and the asymptotic limit A_w is graphically evaluated from Equation (5a).

Having thus extracted time scale T_w and asymptotic limit A_w from the database, the numerical scheme now turns to solving for n+1 unknowns – β_{1w}, β_{2w}, β_{3w}, along with α_w – and to subjecting this solution to satisfy the constraints typified by Equations (4a), (4d), and (5c). As seen from Equation (4d), these n β-coefficients completely determine α_w, not the other way around. Thus, the numerical scheme actually involves the computation of n β-coefficients that satisfy the two constraints given by Equations (4a) and (5c).

Throughout, the constraint given by Equation (4a) is strictly enforced, and the numerical scheme begins with the von Karman model: $\beta_w = 1$. The optimisation algorithm 'sqp' subjected to the constraints detailed above is used to minimise the error between the n β-coefficients of the model and the autospectral data points. When the β coefficients alone are considered without any reference to the asymptotic constraint A_w of Equation (5c). (Recall that Equation (4a) is always enforced), the minimisation process leads to several solutions sets, with minor differences between any two solution sets (e.g. these minor differences are due to the differences in the selection of the autospectral data points.)

When the β coefficients are considered along with the A_w constraint of Equation (5c), the numerical scheme becomes demanding in that it may lead to one set of β-coefficients thus satisfying all the constraints exactly but the β-coefficients may not adequately fit the data. Accordingly, an alternative numerical scheme is devised: A least-squares minimisation of the sum of the errors between the β-coefficients and the autospectral data points and between the A_w coefficient of the model (resulting from the β-coefficients, see Equation (5c)) and the measured A_w. This alternative scheme is found to be remarkably robust and routine, and the computed A_w values are generally found to be within 3%.

https://doi.org/10.1017/aer.2016.47 Published online by Cambridge University Press

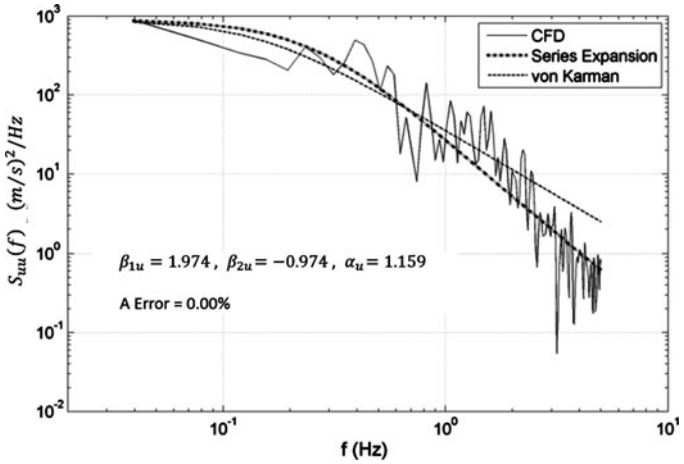


Figure 9. Longitudinal autospectra of airwake-downwash turbulence from CFD, von Karman, and two-term series expansion.

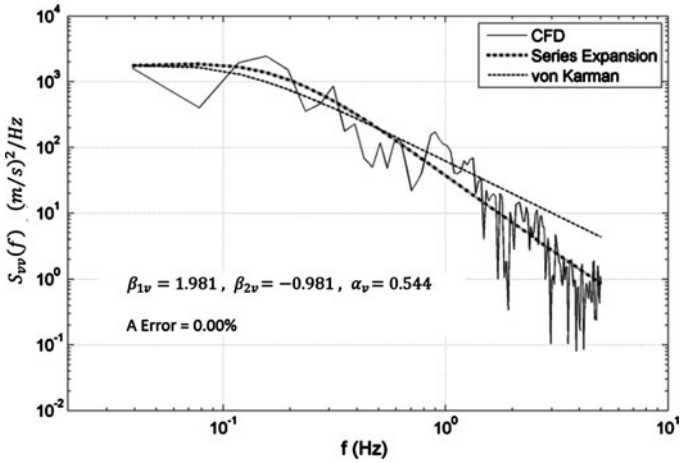


Figure 10. Lateral autospectra of airwake-downwash turbulence from CFD, von Karman, and two-term series expansion.

6.0 AIRWAKE-DOWNWASH MODELS

The framework is tested against a comprehensive database of airwake-downwash turbulence[5]. A representative sample of the results from this testing is now presented in Figs. 9-14. Therein, the extracted interpretive models of autospectra are compared with the numerically generated autospectral data points from the database and the von Karman models (e.g. $\beta_{1u} = 1$ for the longitudinal component).

For a segment of the database, the autospectral data points are found to exhibit a mixed trend: for some velocity components, the Kolmogorov –5/3 Law was clearly exhibited, while for the other components, this Law was not so clearly exhibited. Accordingly, for the same set of autospectral data points, the framework is used with the enforcement of the Kolmogorov Law in Figs. 9-11, and without this enforcement, in Figs. 12-14. Moreover, in Figs. 9-11, "A

https://doi.org/10.1017/aer.2016.47 Published online by Cambridge University Press

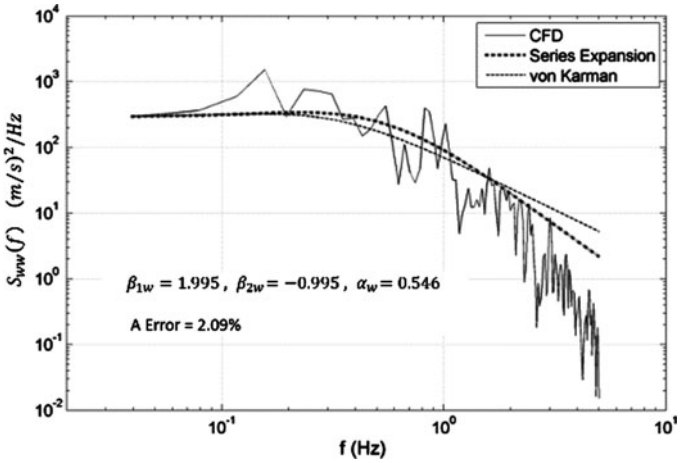


Figure 11. Vertical autospectra of airwake-downwash turbulence from CFD, von Karman, and two-term series expansion.

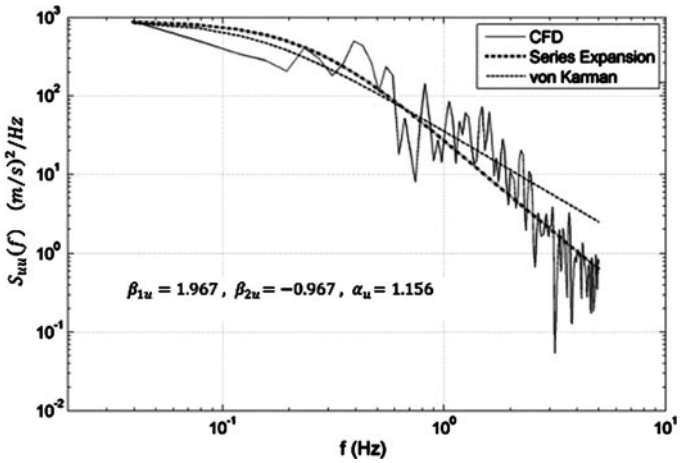


Figure 12. Longitudinal autospectra of airwake-downwash turbulence from CFD, von Karman, and two-term series expansion, without the a-constraint.

Error = xx %" indicates the error in satisfying the Kolmogorov –5/3 Law. As it turns out, rigorous enforcement of Equation (5c) severely limits the model. Due to the nature of the –5/3 law, allowing the model's asymptotic decay level to deviate from the measured value is acceptable. An error of less than 10% is considered acceptable for engineering analysis. To clarify the previous statement: The beta coefficients of Equation (3) are solved for in a least squares (curve fitting) sense, with exact adherence to the constraint Equation (4a). To allow for a greater set of possible solutions, Equation (5c) is enforced to within an acceptable level. Similarly, in Figs. 12-14, "without the A-Constraint" means that the asymptotic decay according to the Kolmogorov –5/3 Law typified by Equation (5c), is not enforced. Now, the least-squares solution is subjected to two constraints, typified by Equations (4a) and (4d). Another point merits mention: The selection of a specific segment of the database with a mixed trend of exhibiting the Kolmogorov –5/3 Law is intentional. Its purpose is to demonstrate

https://doi.org/10.1017/aer.2016.47 Published online by Cambridge University Press

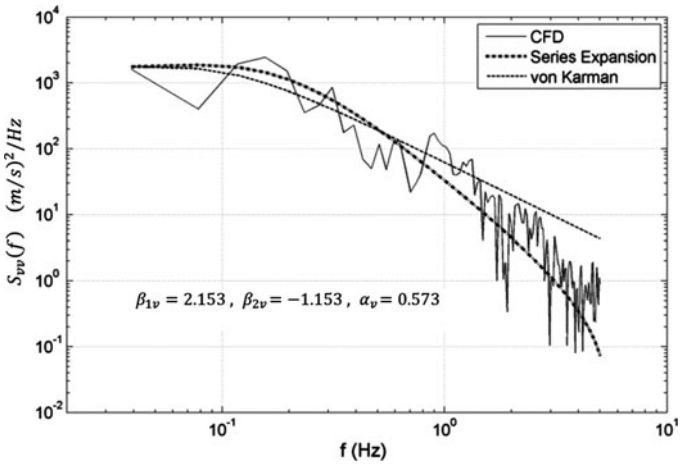


Figure 13. Lateral autospectra of airwake-downwash turbulence from CFD, von Karman, and two-term series expansion without the A-constraint.

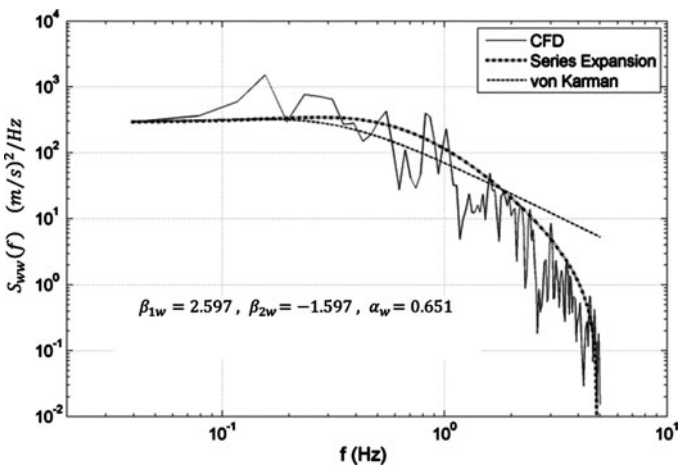


Figure 14. Vertical autospectra of airwake-downwash turbulence from CFD, von Karman, and two-term series expansion without the A-constraint.

that the framework lends itself remarkably well to a wide range of the database, irrespective of whether the autospectral data points exhibit the Kolmogorov –5/3 Law or not. Ignoring Equation (5c) in the model extraction is completely appropriate, if the data itself does not exhibit the –5/3 Law.

As seen from all these six figures, Figs. 9-14, the developed models with only a first-order correction (a two-term series) approximate the autospectral data points remarkably well, and they represent a significant improvement over the von Karman model.

It is also instructive to compare the extracted models with the –5/3 Law enforcement to those without the enforcement. For the longitudinal and lateral components (Figs. 9, 12 and Figs. 10, 13, respectively), the autospectral data points exhibit asymptotic decay according to the –5/3 Law, and enforcement of this Law is found to be desirable. Specifically,

https://doi.org/10.1017/aer.2016.47 Published online by Cambridge University Press

for the longitudinal component, both cases with and without the enforcement lead to virtually identical models, and for the lateral component, the model with the enforcement better approximates the autospectral data points; for example, compare Figs. 10 with 13, in particular, for frequencies greater than 1 Hz.

For the vertical component in Figs. 11 and 14, the autospectral data points exhibit a steeper-than-the –5/3 slope. In this case, the model without this enforcement (Fig. 14) represents a qualitative improvement over the model with the enforcement (Fig. 11). The reason is that the enforcement hinders the framework's capability for the model extraction for the flow-field at this particular location.

In summary, these six figures demonstrate that the framework is remarkably robust: The capability for extracting autospectral models from a wide range of autospectral data points with and without the Kolmogorov –5/3 asymptotic decay. They further demonstrate that, with only a first-order correction, the framework extracts models that provide an excellent approximation of the autospectral data points, and a vast improvement over the von Karman. It is important to note that although the points modelled are below the rotor, they could be applied to any point in the flow field, for example, above and upstream of the rotor.

7.0 SIMULATION FILTERS

For the one-point statistics of autospectrum (e.g. $\tilde{S}_{ww}(f)$ in Equation (3)), simulation requires reconstruction of the random process or time histories from the extracted autospectral models. Accordingly, random white noise is passed through a filter, a single-input single-output system, say with system function $H(f)$. Since white noise autospectrum is constant, it is set to unity, and now, the response autospectrum of the shaping filter is simply $|H(f)|^2$. Thus, the random process reconstruction simplifies to designing a shaping filter with system function $H(f)$ such that $|H(f)|^2$ agrees with the extracted autospectrum model; that is, $\tilde{S}_{ww} = |H(f)|^2$.

A key feature of the extracted autospectrum models of airwake-downwash turbulence, as typified in Equation (3), is that the filter design is virtually identical to the widely-used design for the von Karman autospectra. For the vertical autospectrum, the system function for the extracted autospectrum models can be expressed as[5]:

$$\frac{H_w(f)}{\sigma_W} = \frac{4\sqrt{T_W}\left(1 + b_1 T_W f + b_2 (T_W f)^2\right)}{1 + a_1 T_W f + a_2 (T_W f)^2 + a_3 (T_W f)^3} \quad \ldots (6)$$

In the above equation, T_W is time scale, referred to earlier in Equation (2b). The time scale is calculated from the data. The remaining five coefficients – a_1, a_2, a_3, b_1 and b_2 – are evaluated by nonlinear data fitting to the extracted autospectral model on a least squares basis[5].

7.1 Airwake-Downwash Simulation

The filter design follows Equation (6), and Fig. 15 shows how the autospectra from these white-noise-driven filters compare with the autospectral data points and with the extracted models from the database. These autospectral data points and the extracted models are identical to the models presented earlier in Figs. 9-11. The extracted models are found to lend themselves extremely well to the design of filters[5], and, as seen from Fig. 15, they agree well

https://doi.org/10.1017/aer.2016.47 Published online by Cambridge University Press

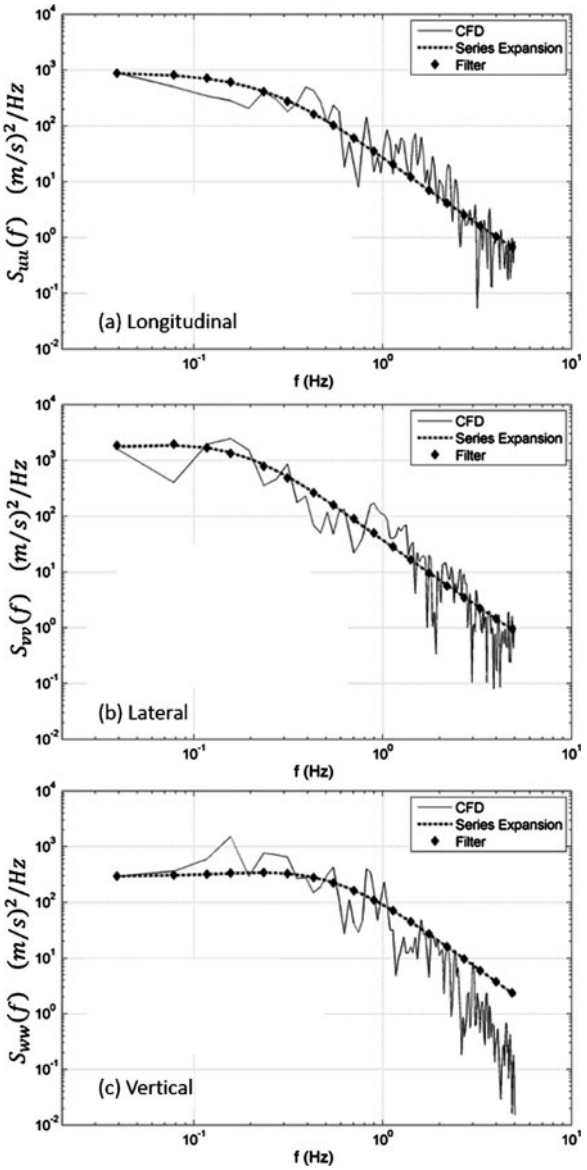


Figure 15. Airwake-downwash turbulence autospectra from CFD, two-term expansion series, and shaping filter simulation of two-term series model.

with the other two sets of models: autospectral data points (CFD) and extracted interpretive model (series expansion).

8.0 CONCLUSIONS

For a better appreciation of these findings, it is emphasised that downwash affects practically all aspects of helicopter shipboard operations, ranging from unsteady fuselage loads to

https://doi.org/10.1017/aer.2016.47 Published online by Cambridge University Press

pilot work load to operational limit[9,10], not to mention the health and safety concerns. Moreover, there is little quantitative information available on the statistical aspects of airwake-downwash coupling. Given this background, this paper's two major contributions are: (1) A quantitative demonstration of the impact of downwash on airwake on the basis of one-point statistics of autospectrum and two-point statistics of cross-spectrum and coherence; these statistics are generated directly from a CFD database for a DDG-81 class ship. The database represents both airwake alone and airwake with downwash and (2) Development of a mathematical framework for extracting autospectral models from a database. Compared to the earlier-exercised series expansion schemes[6–8], the present work develops from first principles the constraint equations in closed-form for time scale and asymptotic decay of the vertical and lateral components. (The corresponding constraints equations for the longitudinal component were developed earlier by Harris[6].) This framework incorporates these time-scale and asymptotic-decay constraints for all three velocity components, and in turn, it ensures that the extracted model captures all three fundamental turbulence characteristics of the autospectral data points: time scale, mean square value and also asymptotic decay according to the Kolmogorov –5/3 Law. Thus, the framework represents a noteworthy advancement over the earlier-proposed series-expansion schemes[6–8].

The framework is tested against a comprehensive database of airwake with downwash, and this testing includes a segment of the database for which the autospectral data points do not clearly exhibit the Kolmogorov –5/3 asymptotic decay. Moreover, the extracted models are further tested as to their suitability for routine simulation through white-noise-driven filters. The one-point and two-point statistics generated directly from the database of airwake and airwake with downwash, and also the framework's application to autospectral modelling, lead to the following specific findings:

1. The one-point statistics of autospectrum (e.g. Fig. 2) show that the airwake energy increases by nearly one order of magnitude and that almost all of this energy is concentrated within the frequency bandwidth of $0.16 \leq f\ (Hz) \leq 1.6$; the bandwidth of concern to flight dynamics. Similarly, the two-point statistics of coherence demonstrate that spectral correlation between the flow-velocity time histories between two points is significantly reduced by downwash coupling.
2. When utilising the presented framework for autospectral model extraction, all that is generally required is a first-order correction (a two-term series). Moreover, the framework is found to be remarkably robust; it lends itself well to a wide range of the database with and without the enforcement of the Kolmogorov –5/3 Law. Stated otherwise, the framework is equally viable for the segment of the database for which the turbulence spectrum does not exhibit the asymptomatic decay according to the –5/3 Law.
3. For the extracted models of autospectrum, the design of the white-noise-driven simulation filters is as routine as the widely used procedure for the von Karman model.

8.1 Future Research

The following points are suggested for future research in the presented area:

1. The database is numerically generated from a CFD-based investigation, in which, the downwash coupling is incorporated through an embedded actuator-disk model, whereas, the flow-field is rapidly distorting and nonlinear, and it involves the interaction of rotor thrust, downwash and airwake as elements in a closed-loop feedback system. Given the

https://doi.org/10.1017/aer.2016.47 Published online by Cambridge University Press

flow-field complexity, a database from wind-tunnel and at-sea experiments, would help validate the current approaches to modelling the fully coupled flow-field of airwake with downwash.

2. The preceding mathematical framework with built-in constraint equations in closed form is restricted to developing interpretive autospectral models of one-point statistics. On the other hand, airwake alone and, more so, airwake with downwash represent nonhomogeneous and distorting flow fields. A relatively complete description of such flows requires both one-point statistics of autospectrum and two-point statistics of cross-spectrum and coherence. Thus, an extension of this framework together with the corresponding constraints in closed form, represents a fruitful area of research.
3. For the one-point statistics of autospectrum, the filter represents a single-input, single-output system driven by white noise; thus the filter design is a routine exercise. Given this background, further research on the feasibility of connecting the extracted autospectral model to a flight simulation code offers promise. For the two-point statistics, the filter represents a multiple-input, multiple-output system. Here as well, further research is required to assess how the interpretive models of these two-point statistics lend themselves to designing such a multiple-input, multiple-output system driven by white noise.
4. Compared to fuselage loads (e.g. drag and yawing moment) induced by airwake alone, the corresponding fuselage loads induced by airwake with downwash are substantially higher[9,10]. Of particular significance is the development of a methodology for incorporating the interpretive models of one-point and two-point statistics as an input matrix in the prediction of these fuselage loads. This methodology would help develop realistic quantitative measures of predicting pilot work load during shipboard operations[10].

ACKNOWLEDGEMENTS

The authors are grateful to the Naval Air Warfare Center Aircraft Division (NAVCAD), Patuxent River, MD, for providing the "CFD Airwake Data for a DDG-81 Class Ship with Embedded H-60 Actuator-Disk Model." The help of Mr. Kuntal Thakkar of Florida Atlantic University, Boca Raton, FL, is gratefully acknowledged as well in the preparation of the paper. The authors are also grateful to Dr. Steven Zan, Director R&D Aerodynamics, NRC Aerospace, Canada, and to Professor Joseph Horn, Pennsylvania State University, PA for reviewing this paper.

REFERENCES

1. GAONKAR, G.H. Review of turbulence modeling and related applications to some problems of helicopter flight dynamics, *J. American Helicopter Society*, January 2008, **53**, (1), pp 87-107.
2. DOANE, S.R. A Wind Tunnel Technique for the Identification of Ship Airwake/Rotor Downwash Coupling, August 2011, PhD Dissertation, Department of Aerospace Engineering, Old Dominion University, Norfolk, Virginia, US, Chapter 2.
3. POLSKY, S.A. and WILKINSON, C.H. A computational study of outwash for a helicopter operating near a vertical face with comparison to experimental data, *AIAA Paper 2009-5684, AIAA Modeling and Simulation Technologies Conference and Exhibit*, 10-13 August 2009, Chicago, Illinois, US.

https://doi.org/10.1017/aer.2016.47 Published online by Cambridge University Press

4. GAONKAR, G.H. On modeling and simulation of airwake and airwake downwash turbulence for helicopter shipboard operations, *American Helicopter Society 69th Annual Forum Proceedings*, 21-23 May 2013, Phoenix, Arizona, US.
5. SCHAU, K. Developing Interpretive Turbulence Models from a Database with Applications to Wind Farms and Shipboard Operations, MSc Thesis, October 2013, Department of Ocean and Mechanical Engineering, Florida Atlantic University, Boca Raton, Florida, US.
6. HARRIS, R.I. Some further thoughts on the spectrum of gustiness in strong winds, *J. Wind Engineering and Industrial Aerodynamics*, 1990, **33**, pp 461-477.
7. GAONKAR, G.H. and MOHAN, R. Extracting stochastic airwake models from a database for engineering analysis and simulation, *J. American Helicopter Society*, April 2012, **57**, (2), pp 1-15.
8. GAONKAR, G.H. Extracting stochastic models of airwake-downwash turbulence from a database for simulation, *J. Aircraft*, 2013, **50**, (4), pp 1309-1311.
9. LEE, R.G. and ZAN, S.J. Wind tunnel testing of a helicopter fuselage and rotor in ship airwake, *Journal of the American Helicopter Society*, October 2005, **50**, (4), pp 326-337.
10. ZAN, S.J. On aerodynamic modelling and simulation of the dynamic interface, *Proceedings of the Institution of Mechanical Engineers, Part G; J Aerospace Engineering*, 1 May 2005, **219**, (5), pp 393-410.
11. MATHIEU, J. and SCOTT, J. Chapters 6: Spectral analysis of homogeneous turbulence and Chapter 7: Kolmogorov's and other theories based on spectral analysis, *An Introduction to Turbulent Flow*, 2000, Cambridge University Press, New York, New York, US, pp 239-282; 283-326.
12. TOWNSEND, A.A. Chapter 3: Homogenous turbulent flows, *The Structure of Turbulent Shear Flow*, 2nd ed., 1976, Cambridge University Press, New York, New York, US, pp 45-104.
13. BENDAT, J.S. and PIERSOL, A.G. Chapter 5: Stationary Random Processes, *Random Data, Analysis and Measurement Procedures*, 3rd ed., 2000, John Wiley and Sons, New York, New York, US, pp 118-188.
14. SIMIU, E. and SCANLAN, R.H. Chapter 2: The Atmospheric Boundary Layer, *Wind Effects on Structures*, 3rd ed., 1996, John Wiley and Sons, Inc., New York, New York, US, pp 33-90.

https://doi.org/10.1017/aer.2016.47 Published online by Cambridge University Press